Bearing-Only Navigation with Field of View Constraints

Arman Karimian and Roberto Tron

***Abstract*—This paper addresses the problem of navigation using only relative directional measurements (i.e., relative distances are unknown) with field of view constraints. We present a novel navigation vector field for the bearing-based visual homing problem with respect to static landmarks in 2-D and 3-D environments. Our method employs two control fields that are tangent and normal to ellipsoids having landmarks as their foci. The tangent field steers the robot to a set of points where the average of observed bearing vectors is parallel to the average of the desired bearings. The normal field uses the angle between different pairs of bearings as a proxy to adjust the robot's distance from the landmarks and to satisfy the field of view constraints. Both fields are blended together to construct an almost globally stable control law. Our method is straightforward to implement, as it requires only comparisons between average bearings, and angles of pairs of vectors. We provide simulations that demonstrate the robustness of our approach on two systems: a double integrator, and a unicycle.**

***Index Terms*—visual homing, field of view constraint, bearing-only navigation, navigation vector field**

I. INTRODUCTION

Control in robotic systems is an ongoing research area. One interesting problem is bearing-only navigation, which is motivated by the use of vision sensors in robotics applications. Vision sensors, such as monocular cameras, can provide accurate bearing (relative direction) measurements, although the corresponding distances are typically difficult to obtain with comparable precision. In addition, vision sensors typically have a limited field of view (FOV). These two limitations increases the complexity of bearing-only navigation considerably.

The problem addressed here is visual homing: the task of reaching a desired location using the bearing measurements of fixed landmarks in the environment [7]. A practical application of this problem is when a robot takes a picture of the environment from a home location, moves to a new location, and then needs to return to the home location using only visual data from the camera. Existing methods can be divided into gradient methods [4], [12], [22], image-based visual servoing [3], [15], [20], and ad-hoc methods [1], [13], [14], [16]. While gradient methods can achieve global stability [22] without using range estimation (actual or estimated), FOV constraints are not generally considered in any of these methods, and it is common to assume omnidirectional vision sensors. Notable exceptions are [17] where a homography-based approach is given for keeping a single target in the field of view of a unicycle with an onboard IMU and with a camera attached to the body, and [4] where a navigation function based approach was used but required planar targets with known geometry.

The authors are with the Department of Mechanical Engineering, Boston University, Boston, MA. E-mail: {armandok,tron}@bu.edu.

FOV constraints restrict the feasible locations for the moving sensor carried by the robot, thus effectively creating obstacles in the configuration space of the robot. To complete the visual homing task the robot must avoid these obstacles to not lose track of objects of interest; however, the locations of such obstacles is not directly available to the robot, due to lacking distance measurements. Many different methods have been suggested for control-based obstacle avoidance, some of which are potential methods [6], [10], navigation functions [21], and harmonic functions [2], [11]. Potential methods are prone to local minima; navigation functions are free of local minima but are sensitive to the value of a tuning parameter which is not known a priori, and harmonic functions are usually computationally demanding and require the location of the obstacles. An alternative approach is to directly design a *navigation vector field* which encodes the objectives (desired home location and FOV obstacle avoidance), and is employed directly or indirectly in the control synthesis step. This idea was used for obstacle avoidance in unicycles, but with *full information on the relative position of the robot and obstacles* [18], [19].

Our approach. We introduce two orthogonal flows that respectively adjust the direction of the average of the bearings and the angle between a pair of bearings. We then combine these two flows into a navigation flow, which is used to design controllers for solving the visual homing problem in the presence of FOV constraints. Our approach is applicable to both 2-D and 3-D environments, and presents almost-global convergence for single integrators. We use this navigation field to design controllers for damped double integrators and unicycles. To the best of our knowledge, no other method exists that tackles FOV constraints without knowledge about landmark positions. Our approach does not rely on all of the bearings directly, rather uses the normalized average of the bearings and a single angle between two non-collinear bearings. We assume that the camera on the robot can rotate independently from the body and direction of motion of the robot, and we model the field of view as a cone with angle less than π. Additionally, we assume that the robot's local reference frame is axis-aligned with a fixed world frame (e.g., through a global compass direction).

II. NOTATION AND PRELIMINARIES

We denote the dimension of the workspace by $d \in \{2, 3\}$. The *bearing measurement* is a unit vector given by:

$$\mathbf{u}(\mathbf{a}, \mathbf{b}) \doteq \frac{\mathbf{b} - \mathbf{a}}{\|\mathbf{b} - \mathbf{a}\|}, \tag{1}$$

where $\mathbf{a}, \mathbf{b} \in \mathbb{R}^d$ are distinct. We denote the cardinality of a discrete set $\mathcal{P}$ as $|\mathcal{P}|$, and the boundary of a continuous set $\mathcal{Q}$ as $\partial\mathcal{Q}$. The identity matrix is denoted by $\mathbf{I}_d \in \mathbb{R}^{d\times d}$, the

d-dimensional unit sphere by $\mathbb{S}^d$, the Minkowski sum by $\oplus$, and proportionality by $\propto$. We use $\measuredangle(\mathbf{u}_1, \mathbf{u}_2)$ to denote the (non-oriented) angle in radians between two vectors $\mathbf{u}_1, \mathbf{u}_2$. A *projection matrix* $\mathbf{P}(\mathbf{v}) \in \mathbb{R}^{d\times d}$ for $\mathbf{v} \in \mathbb{R}^d$ is defined by:

$$\mathbf{P}(\mathbf{v}) \doteq \mathbf{I}_d - \frac{\mathbf{v}\mathbf{v}^\mathsf{T}}{\|\mathbf{v}\|^2}; \tag{2}$$

$\mathbf{P}(\mathbf{v})$ is symmetric, positive semidefinite, with a zero eigenvalue corresponding to $\mathbf{v}$, while other eigenvalues are one.

Given k fixed and distinct points $\mathcal{P} = \{\mathbf{p}_i\}_{i=1}^k$ in $\mathbb{R}^d$, we define the *distance function* $\vartheta_\mathcal{P}(\mathbf{x}) \doteq \sum_{i=1}^k \|\mathbf{x} - \mathbf{p}_i\|$ to be the sum of distances from $\mathbf{x}$ to all points in $\mathcal{P}$. We have the following facts regarding the function $\vartheta_\mathcal{P}$.

Definition 1. *A* k-ellipsoid *is the set of points over which* $\vartheta_\mathcal{P}(\cdot)$ *is equal to a constant* r*, and points in* $\mathcal{P}$ *are called* foci*. Equivalently, it is the boundary of the set-valued map:*

$$\mathcal{Q}(r) = \{\mathbf{x} \in \mathbb{R}^d : \vartheta_\mathcal{P}(\mathbf{x}) \leq r\}. \tag{3}$$

Lemma 1. *The Jacobian of a unit vector* $\mathbf{z} = \frac{\boldsymbol{g}(\mathbf{x})}{\|\boldsymbol{g}(\mathbf{x})\|} \in \mathbb{R}^d$ *with respect to* $\mathbf{x} \in \mathbb{R}^d$ *is given by:* $\|\boldsymbol{g}(\mathbf{x})\|^{-1}\mathbf{P}(\boldsymbol{g}(\mathbf{x}))\frac{\partial \boldsymbol{g}}{\partial \mathbf{x}}$.

Proof. Since $\frac{\partial \mathbf{z}}{\partial \mathbf{x}} = \|\boldsymbol{g}(\mathbf{x})\|^{-1}\frac{\partial \boldsymbol{g}}{\partial \mathbf{x}} + \|\boldsymbol{g}(\mathbf{x})\|^{-3}\boldsymbol{g}\boldsymbol{g}^\mathsf{T}\frac{\partial \boldsymbol{g}}{\partial \mathbf{x}}$, the proof is complete by collecting $\|\boldsymbol{g}(\mathbf{x})\|^{-1}$ and $\frac{\partial \boldsymbol{g}}{\partial \mathbf{x}}$. □

Lemma 2. *The Hessian of* $\vartheta_\mathcal{P}$ *is positive semidefinite, and is positive definite if all points in* $\mathcal{P}$ *are not collinear.*

Proof. We have $\frac{\partial \vartheta_\mathcal{P}}{\partial \mathbf{x}} = -\sum_{i=1}^k \mathbf{u}(\mathbf{x}, \mathbf{p}_i)$, $\mathbf{H}(\mathbf{x}) \doteq \frac{\partial^2 \vartheta_\mathcal{P}}{\partial \mathbf{x}^2} = \sum_{i=1}^k \frac{\mathbf{P}(\mathbf{u}(\mathbf{x},\mathbf{p}_i))}{\|\mathbf{x}-\mathbf{p}_i\|}$. Since $\mathbf{H}$ is the sum of positive semidefinite projection matrices, $\mathbf{H}$ is also positive semidefinite. Moreover, we have $\mathbf{w}^\mathsf{T}\mathbf{H}\mathbf{w} = \mathbf{0}$ for some $\mathbf{w}$, and hence $\mathbf{H}$ is positive semi-definite if and only if each term in the sum has the same eigenvector with zero eigenvalue, i.e., all the points in $\mathcal{P} \cup \mathbf{x}$ are collinear. In all other cases, $\mathbf{H}$ is positive definite. □

A point $\mathbf{p} \in \mathbb{R}^d$ is said to be a *geometric median* of $\mathcal{P}$ if $\mathbf{p} \in \operatorname{argmin}_\mathbf{x} \vartheta_\mathcal{P}(\mathbf{x})$. We have $\frac{\partial \vartheta_\mathcal{P}}{\partial \mathbf{x}}(\mathbf{p}) = \mathbf{0}$ if $\mathbf{p} \notin \mathcal{P}$.

Lemma 3 ([23])**.** *The geometric median of* $\mathcal{P}$ *is unique, unless all points in* $\mathcal{P}$ *are collinear and* k *is even.*

Definition 2. *The normalized vector field* $\boldsymbol{f}(\cdot)$ *is denoted as* $\boldsymbol{f}^\circ \doteq \frac{\boldsymbol{f}}{\|\boldsymbol{f}\|}$*, with* $\boldsymbol{f}^\circ = \mathbf{0}$ *if* $\|\boldsymbol{f}\| = 0$ *or* $\boldsymbol{f}$ *is undefined.*

III. BEARING-ONLY NAVIGATION

The goal in the *visual homing problem* is to steer a robot to a *desired location* $\mathbf{x}^* \in \mathbb{R}^d$, specified by a set of (measured) *desired relative bearings* with respect to some *fixed landmarks* in the environment with *unknown locations*. In addition, the robot can only measure its *relative bearings* of the landmarks. More formally, assuming there are a total of k landmarks $\mathcal{P} = \{\mathbf{p}_i \in \mathbb{R}^d\}_{i=1}^k$ present with $k \geq 2$, the desired bearings are given by $\{\mathbf{u}_i^*\}_{i=1}^k$ where $\mathbf{u}_i^* \doteq \mathbf{u}(\mathbf{x}^*, \mathbf{p}_i)$, and measured relative bearings are given by $\{\mathbf{u}_i\}_{i=1}^k$ where $\mathbf{u}_i \doteq \mathbf{u}(\mathbf{x}, \mathbf{p}_i)$ and $\mathbf{x} \in \mathbb{R}^d$ is the current location of the robot.

In the presence of FOV restrictions and absence of information about landmark locations, the robot must be able to maintain its sight over the landmarks and use the measured bearings to reach the goal position. Losing sight of them might make it hard to recover as the robot has to readjust its position to some feasible location, but finding such position requires some knowledge over the whereabouts of $\mathcal{P}$. To avoid this dilemma, we enforce the following conditions:

$$\measuredangle(\mathbf{u}_i, \mathbf{u}_j) \leq \phi_{\text{FOV}}, \quad \forall i, j \in \{1, \ldots, k\}. \tag{4}$$

The constraints in (4) ensure that all the landmarks remain in the visual field of the robot's camera, modeled as a cone with angle $\phi_{\text{FOV}} < \pi$. This can be summarized as $\mathbf{x}(t) \notin \bigcup_{i,j} \mathcal{O}_{ij}$ for all t, where $\mathcal{O}_{ij}$ is a *field of view obstacle* set defined as:

$$\mathcal{O}_{ij} \doteq \{\mathbf{x} \in \mathbb{R}^d : \measuredangle(\mathbf{u}_i, \mathbf{u}_j) > \phi_{\text{FOV}}\}. \tag{5}$$

Using this definition, we rewrite the problem statement as:

Problem 1. *Given a set of desired bearings* $\{\mathbf{u}_i^*\}_{i=1}^k$ *of* $k \geq 2$ *fixed landmarks* $\mathcal{P}$*, find a controller that steers the robot to the desired position where* $\mathbf{u}_i = \mathbf{u}_i^*$*,* $\forall i$ *using only bearing measurements* $\{\mathbf{u}_i\}_{i=1}^k$ *while avoiding all* $\mathcal{O}_{ij}$ *sets.*

We make these assumptions in solving this problem: *1)* The robot carries a *rotating camera*, e.g. a conventional camera mounted on a servo motor, which rotates freely from the movement of robot. *2)* The robot has perfect *knowledge of orientation*, i.e. it knows the orientations of its body frame and the camera with respect to some global frame and hence the measured current bearings and desired bearings are all given in a common orientation frame. *3)* The measured bearings are always *correctly matched* with the corresponding landmarks.

In this section, we introduce two vector fields we use to respectively adjust the robot's distance from the landmarks and direction of the average bearing vector. Later, we combine them into our navigational vector field and use it for control synthesis. We also provide analysis on the performance of this field when the last two assumptions are not met.

A. Normal Flow

To avoid losing track of the landmarks, we require that the robot avoid entering obstacle sets $\mathcal{O}_{ij}$. Instead of directly enforcing this, we achieve this by forcing the robot to stay in a *safe set*. We use the fact that the goal position $\mathbf{x}^*$ is feasible w.r.t. (4) and the pairwise angles between the desired bearings, i.e. $\measuredangle(\mathbf{u}_i^*, \mathbf{u}_j^*)$, are all less than ϕ_{FOV}. We define *desired safe* sets as regions where the view angle of landmarks is less than or equal to the desired view angle given by desired bearings:

$$\mathcal{D}_{ij}^* \doteq \{\mathbf{x} \in \mathbb{R}^d : \measuredangle(\mathbf{u}_i, \mathbf{u}_j) \leq \measuredangle(\mathbf{u}_i^*, \mathbf{u}_j^*)\},\ \mathcal{D}^* \doteq \bigcap_{i,j} \mathcal{D}_{ij}^*. \tag{6}$$

By definition, the set $\mathcal{D}^*$ and obstacle sets $\mathcal{O}_{ij}$ are disjoint and therefore staying in $\mathcal{D}^*$ will guarantee FOV obstacle avoidance. This notion is depicted in Fig. 1a for $d = 2$. For $d = 3$, $\mathcal{O}_{ij}$ and $\mathcal{D}_{ij}^*$ can be visualized by revolving their 2-D version about the line intersecting with $\mathbf{p}_i$ and $\mathbf{p}_j$.

Moreover, it follows that $\mathbf{x}^* \in \mathcal{D}^*$. In fact, since $\mathbf{x}^*$ is located on the boundary of $\mathcal{D}_{ij}^*$ and $\mathcal{D}^*$ is formed by the intersection of such sets, we have $\mathbf{x}^* \in \partial\mathcal{D}^*$. This fact motivates the design of a vector field that *converges to* $\partial\mathcal{D}^*$. For this purpose, we

define the *normalized sum* of the current and desired bearings by:

$$\mathbf{v}(\mathbf{x}) \doteq \frac{\sum_{i=1}^{k} \mathbf{u}_i}{\|\sum_{i=1}^{k} \mathbf{u}_i\|}, \quad \mathbf{v}^* \doteq \frac{\sum_{i=1}^{k} \mathbf{u}_i^*}{\|\sum_{i=1}^{k} \mathbf{u}_i^*\|} = \mathbf{v}(\mathbf{x}^*). \tag{7}$$

Notice that $\mathbf{v}$ is a vector field and $\mathbf{v}^*$ is a fixed vector.

Remark 1. *The vector $\mathbf{v}$ is defined everywhere, except at the landmarks (i.e. $\mathbf{x} = \mathbf{p}_i$ where $\mathbf{u}_i$ is undefined), and where the gradient of $\vartheta_{\mathcal{P}}$ is zero ($-\sum_{i=1}^{k} \mathbf{u}_i = \mathbf{0}$), which happens at the geometric median of the landmarks. The geometric median is a unique point unless k is even and all foci are collinear (e.g. an ellipse), then $\mathbf{v}$ is not defined on the line segment that contains the two middle foci (Lemma 3).*

We also define δ_{ij} to be the difference of the cosine of the current and desired bearings of landmarks $\mathbf{p}_i$ and $\mathbf{p}_j$:

$$\delta_{ij}(\mathbf{x}) \doteq \mathbf{u}_i^{\mathsf{T}} \mathbf{u}_j - \mathbf{u}_i^{*\mathsf{T}} \mathbf{u}_j^*. \tag{8}$$

Note that $\mathcal{D}_{ij}^*$ can be redefined as $\{\mathbf{x} \in \mathbb{R}^d : \delta_{ij}(\mathbf{x}) \geq 0\}$.

Now, we present our *normal field* $\boldsymbol{f}_n$ as:

$$\boldsymbol{f}_n(\mathbf{x}) \doteq \operatorname{sign}(\delta_{\hat{\imath}\hat{\jmath}})\mathbf{v}, \tag{9}$$

where indices $\hat{\imath}$ and $\hat{\jmath}$ are chosen as:

$$\hat{\imath}, \hat{\jmath} \doteq \underset{\substack{i,j \\ \mathbf{u}_i^* \neq \mathbf{u}_j^*}}{\operatorname{argmin}} \delta_{ij}. \tag{10}$$

The condition $\mathbf{u}_i^* \neq \mathbf{u}_j^*$ in (10) excludes the case where $\mathbf{x}^*, \mathbf{p}_i, \mathbf{p}_j$ are collinear, in which case the $\mathcal{D}_{ij}^*$ becomes degenerate (the line containing $\mathbf{p}_i$ and $\mathbf{p}_j$ except the line segment $\mathbf{p}_i$-$\mathbf{p}_j$). In practice, this means landmarks are occluding each other, and it would be impossible to differentiate them.

The sign of $\delta_{\hat{\imath}\hat{\jmath}}$ determines whether the robot is in $\mathcal{D}^*$ or not. If $\delta_{\hat{\imath}\hat{\jmath}} < 0$, then the robot is outside of at least one of the pairwise safe sets $\mathcal{D}_{ij}^*$ and therefore is not in $\mathcal{D}^*$. Otherwise if $\delta_{\hat{\imath}\hat{\jmath}} \geq 0$, we have $\mathbf{x} \in \mathcal{D}^*$, with equality holding on $\partial\mathcal{D}^*$. The normal field $\boldsymbol{f}_n$ moves the robot away from the landmarks if the robot is not in $\mathcal{D}^*$, and moves it towards the landmarks if the robot is in the interior of $\mathcal{D}^*$ (see Fig.1b and Fig.1c).

Theorem 1. *The normal flow $\boldsymbol{f}_n(\mathbf{x})$ converges to $\partial\mathcal{D}^*$.*

Proof. Take the Lyapunov function $V_n = \frac{1}{2}\|\sum_{i=1}^{k} \mathbf{u}_i\|^2$. By expanding V_n, we get $V_n = \frac{k}{2} + \sum_{i<j} \mathbf{u}_i^{\mathsf{T}} \mathbf{u}_j$, which is the sum of cosine of pairwise angles between the bearings with $\frac{k}{2}$. Hence, $\frac{\partial V_n}{\partial \mathbf{x}} = -\sum_{i<j} \left(\frac{\mathbf{P}(\mathbf{u}_i)}{\|\mathbf{x}-\mathbf{p}_i\|} \mathbf{u}_j + \frac{\mathbf{P}(\mathbf{u}_j)}{\|\mathbf{x}-\mathbf{p}_j\|} \mathbf{u}_i \right)$. As $\forall \mathbf{w} : \mathbf{P}(\mathbf{w})\mathbf{w} = \mathbf{0}$, we have $\frac{\partial V_n}{\partial \mathbf{x}} = -\sum_{i<j} (\frac{\mathbf{P}(\mathbf{u}_i)}{\|\mathbf{x}-\mathbf{p}_i\|} + \frac{\mathbf{P}(\mathbf{u}_j)}{\|\mathbf{x}-\mathbf{p}_j\|})(\mathbf{u}_i + \mathbf{u}_j) = -\frac{1}{2}(\sum_{i=1}^{k} \frac{\mathbf{P}(\mathbf{u}_i)}{\|\mathbf{x}-\mathbf{p}_i\|})(\sum_{i=1}^{k} \mathbf{u}_i)$. By factoring out the Hessian (Lemma 2), we get $\dot{V}_n = \frac{\partial V_n}{\partial \mathbf{x}}^{\mathsf{T}} \dot{\mathbf{x}} = -\frac{1}{2}\left(\sum_{i=1}^{k} \mathbf{u}_i\right)^{\mathsf{T}} \mathbf{H} \dot{\mathbf{x}}$. If $\delta_{\hat{\imath}\hat{\jmath}} > 0$ and hence $\dot{\mathbf{x}} = \mathbf{v}$, we have $\dot{V}_n < 0$ almost everywhere (except at geometric median or if all landmarks are collinear) and decrease in V_n means an overall increase in the pairwise angles. The opposite is true for $\delta_{\hat{\imath}\hat{\jmath}} < 0$. In addition, $\partial\mathcal{D}^*$ is a bounded and closed surface, hence following $\boldsymbol{f}_n$ (which adjusts $\vartheta_{\mathcal{P}}$ and spans entire $\mathbb{R}^d$) eventually leads to $\partial\mathcal{D}^*$. □

Despite the overall reduction of pairwise angles when the robot moves away from landmarks, if the robot has a small field of view (i.e. ϕ_{FOV} is small) and starts outside of $\mathcal{D}^*$ and very close to landmarks, it might briefly enter an obstacle set on its way towards $\mathcal{D}^*$. Even if this happens, one remedy would be to keep moving away in the same direction until the landmarks are back in sight.

B. Tangential Flow

We previously defined the safe set $\mathcal{D}^*$ and the normal field $\boldsymbol{f}_n$ which converges to $\partial\mathcal{D}^*$ containing $\mathbf{x}^*$. Here we introduce

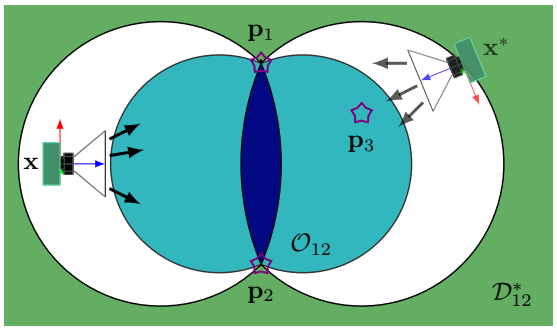

(a) Obstacle set $\mathcal{O}_{12}$ for $\phi_{\text{FOV}} \in \{\frac{3\pi}{8}, \frac{7\pi}{8}\}$ and the desired safe set $\mathcal{D}_{12}^*$. Boundaries are shown in black.

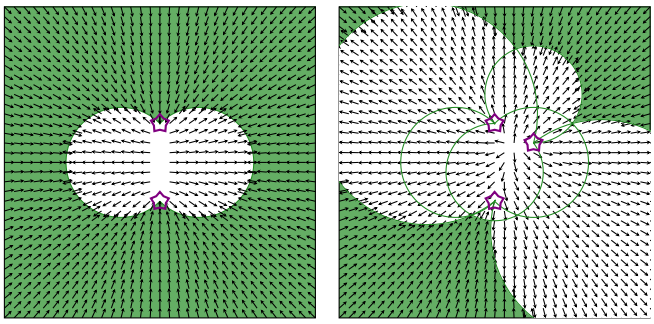

(b) $\boldsymbol{f}_n^\circ(\mathbf{x}), k = 2$ (c) $\boldsymbol{f}_n^\circ(\mathbf{x}), k = 3$

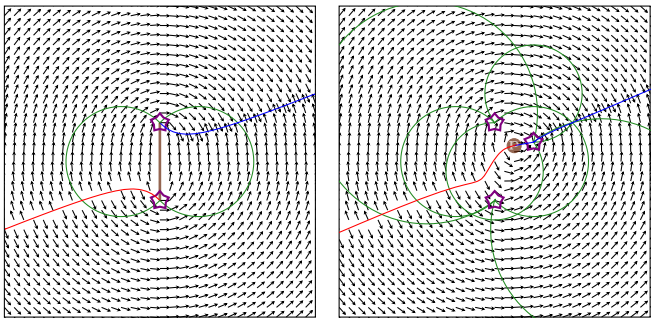

(d) $\boldsymbol{f}_t^\circ(\mathbf{x}), k = 2$ (e) $\boldsymbol{f}_t^\circ(\mathbf{x}), k = 3$

Figure 1: (a) shows the current and goal positions $\mathbf{x}, \mathbf{x}^*$, three landmarks (⬠), and the $\mathcal{O}_{12}$ and $\mathcal{D}_{12}^*$ sets. In (b)-(c) the normal flow $\boldsymbol{f}_n^\circ$ and the set $\mathcal{D}^*$ are shown for two and three landmarks, and in (d)-(e) the tangential flow $\boldsymbol{f}_t^\circ$ and the isonormal curves $\boldsymbol{\xi}_{\mathbf{v}^*}$ and $\boldsymbol{\xi}_{-\mathbf{v}^*}$ are observed. The goal position $\mathbf{x}^*$ is at the intersection of the $\partial\mathcal{D}^*$ set and the $\boldsymbol{\xi}_{\mathbf{v}^*}$ curve. Since there are an even number of collinear landmarks in (d), geometric median is not unique and is shown by the line segment $\mathbf{p}_1$-$\mathbf{p}_2$. In (e) geometric median is unique and is shown by ●.

a complementary field which also contains $\mathbf{x}^*$ as an equilibrium point. The *tangential field* $\boldsymbol{f}_t$ is defined as:

$$\boldsymbol{f}_t(\mathbf{x}) = -\mathbf{P}(\mathbf{v})\mathbf{v}^*. \tag{11}$$

Contrary to $\boldsymbol{f}_n$, $\boldsymbol{f}_t$ keeps the value of $\vartheta_{\mathcal{P}}$ fixed.

Lemma 4. *The two vector fields $\boldsymbol{f}_t$ and $\boldsymbol{f}_n$ are orthogonal and integral curves of $\boldsymbol{f}_t$ lie on k-ellipsoids.*

Proof. Since $\mathbf{v}^\mathsf{T}\mathbf{P}(\mathbf{v}) = \mathbf{v}^\mathsf{T}(\mathbf{I}_d - \mathbf{v}\mathbf{v}^\mathsf{T}) = \mathbf{0}$, we have $\boldsymbol{f}_n^\mathsf{T}\boldsymbol{f}_t = 0$ everywhere. Moreover, $\boldsymbol{f}_t$ is always orthogonal to $\mathbf{v}$ and therefore orthogonal to the gradient of $\vartheta_{\mathcal{P}}(\mathbf{x})$, ergo moving with $\boldsymbol{f}_t$ does not change $\vartheta_{\mathcal{P}}$, hence the claim. While $\boldsymbol{f}_n$ is always parallel to the gradient of $\vartheta_{\mathcal{P}}(\mathbf{x})$ and therefore *normal* to k-ellipsoids, $\boldsymbol{f}_t$ is always *tangent* to k-ellipsoids. □

Plots of the normalized tangential field are given in Figures 1d-1e, which shows that the flows lie on 2-ellipsoids (i.e. ellipses) and 3-ellipsoids. Additionally, $\boldsymbol{f}_t$ circumvents the landmarks instead of directly passing between them. This behavior is useful for avoiding FOV obstacles sets.

Here we show that $\boldsymbol{f}_t$ yields convergence of $\mathbf{v}$ to $\mathbf{v}^*$. Later, we investigate its equilibrium points and their properties.

Theorem 2. *The flow $\dot{\mathbf{x}} = \boldsymbol{f}_t(\mathbf{x})$ leads to convergence of $\mathbf{v}$ to $\mathbf{v}^*$ almost globally.*

Proof. Take $V_t = \frac{1}{2}\|\mathbf{v} - \mathbf{v}^*\|^2$ as a Lyapunov function. Using the chain rule, $\frac{\partial V_t}{\partial \mathbf{x}} = (\mathbf{v} - \mathbf{v}^*)^\mathsf{T}\frac{\partial \mathbf{v}}{\partial \mathbf{x}}$ and $\frac{\partial \mathbf{v}}{\partial \mathbf{x}} = \|\sum_{i=1}^k \mathbf{u}_i\|^{-1}\mathbf{P}(\sum_{i=1}^k \mathbf{u}_i)\frac{\partial \sum_{i=1}^k \mathbf{u}_i}{\partial \mathbf{x}}$ (Lemma 1). From Lemma 2, we have $\frac{\partial \sum_{i=1}^k \mathbf{u}_i}{\partial \mathbf{x}} = -\mathbf{H}$, where $\mathbf{H}$ is the Hessian of $\vartheta_{\mathcal{P}}$. Also from (2) we have $\mathbf{P}(\sum_{i=1}^k \mathbf{u}_i) = \mathbf{P}(\mathbf{v})$. Hence, $\dot{V}_t = \frac{\partial V_t}{\partial \mathbf{x}}\dot{\mathbf{x}} = \|\sum_{i=1}^k \mathbf{u}_i\|^{-1}(\mathbf{v} - \mathbf{v}^*)^\mathsf{T}\mathbf{P}(\mathbf{v})\mathbf{H}\mathbf{P}(\mathbf{v})\mathbf{v}^*$. Since $\mathbf{v}^\mathsf{T}\mathbf{P}(\mathbf{v}) = \mathbf{0}$ and $\mathbf{P}(\cdot)$ is symmetric, we can simplify the expression for $\dot{V}_t$ as $\dot{V}_t = -\|\sum_{i=1}^k \mathbf{u}_i\|^{-1}\boldsymbol{f}_t^\mathsf{T}\mathbf{H}\boldsymbol{f}_t$. Using Lemma 2, if $\mathbf{H}$ is positive definite we have $\dot{V} < 0$ whenever $\boldsymbol{f}_t \neq \mathbf{0}$. If $\mathbf{H}$ is positive semidefinite, $\mathbf{v}$ is also parallel to all bearings and the zero eigenvector of $\mathbf{H}$, and because $\boldsymbol{f}_t$ is orthogonal to $\mathbf{v}$ (see Lemma 4) we again have $\dot{V} < 0$. However, we have $\boldsymbol{f}_t = \mathbf{0}$ if $\mathbf{v} = \pm\mathbf{v}^*$. This means that any point $\mathbf{x}_0$ with $\mathbf{v}(\mathbf{x}_0) = -\mathbf{v}^*$ is an unstable equilibrium point of $\boldsymbol{f}_t$. □

To find the equilibrium points of $\boldsymbol{f}_t$, we need to find points where $\mathbf{v}(\mathbf{x}) = \pm\mathbf{v}^*$, since $\mathbf{P}(\mathbf{v}^*)\mathbf{v}^* = \mathbf{P}(-\mathbf{v}^*)\mathbf{v}^* = \mathbf{0}$. We will show that such points form two curves $\{\boldsymbol{\xi}_{\mathbf{v}^*}, \boldsymbol{\xi}_{-\mathbf{v}^*}\}$, which we call *isonormal curves*, and they start from a/the geometric median point of the foci and move away from the foci such that they intersect with any k-ellipsoid only once.

Proposition 1. *Let $\boldsymbol{\xi}_{\mathbf{v}_0} = \{\mathbf{x} \in \mathbb{R}^d : \mathbf{v}(\mathbf{x}) = \mathbf{v}_0\}$ be the set of points where $\mathbf{v}$ is equal to a value $\mathbf{v}_0 \in \mathbb{S}^{d-1}$. Then:*

1) *$\boldsymbol{\xi}_{\mathbf{v}_0}$ is a 1-D open curve.*
2) *Focus $\mathbf{p}_i$ belongs to $\boldsymbol{\xi}_{\mathbf{v}_0}$ if $\mathbf{v}_0 \in \mathcal{U}_i$, where*

$$\mathcal{U}_i \doteq \{\frac{\mathbf{e}}{\|\mathbf{e}\|} : \mathbf{e} \in \sum_{j\neq i} \mathbf{u}(\mathbf{p}_i, \mathbf{p}_j) \oplus \mathbb{S}^{d-1}\}. \tag{12}$$

3) *Every point in $\boldsymbol{\xi}_{\mathbf{v}_0} \setminus \mathcal{P}$ is regular.*

Proof. The proof is based on compactness and strict convexity of the set $\mathcal{S} = \mathcal{Q}(r)$ [8, Proposition 4]. Considering only hyperplanes with normal vector $\mathbf{v}_0$ toward the inside of $\mathcal{S}$ (opposite of gradient of $\vartheta_{\mathcal{P}}$), for a given r the hyperplane is tangent at exactly one point on $\mathcal{S}$; equivalently stated, the Gauss map [5] of $\mathcal{S}$ (i.e. $\partial\mathcal{S} \mapsto \mathbb{S}^{d-1}$) is surjective. Uniqueness of the normal vector $\mathbf{v}_0$ on $\mathcal{S}$ implies that $\boldsymbol{\xi}_{\mathbf{v}_0}$ intersects with any k-ellipsoid ($\partial\mathcal{S}$) at a single point. Starting from $r_{\min} = \min_{\mathbf{x}} \vartheta_{\mathcal{P}}(\mathbf{x})$ which happens at a/the geometric median point, as $r \to \infty$ the set $\boldsymbol{\xi}_{\mathbf{v}_0}$ traces a curve which we now show to be regular everywhere except at the foci. Let $\boldsymbol{\zeta}(r) \in \boldsymbol{\xi}_{\mathbf{v}_0}$ represent the point on $\partial\mathcal{S}$ with $\mathbf{v}(\boldsymbol{\zeta}) = \mathbf{v}_0$ and $\vartheta_{\mathcal{P}}(\boldsymbol{\zeta}) = r$. By definition, for all r we have $\boldsymbol{\eta}(r) \doteq \sum_{i=1}^k \mathbf{u}(\boldsymbol{\zeta}(r), \mathbf{p}_i) \propto \mathbf{v}_0$, and therefore $\frac{\partial}{\partial r}\boldsymbol{\eta} = \frac{\partial \boldsymbol{\eta}}{\partial \boldsymbol{\zeta}}\frac{\partial \boldsymbol{\zeta}}{\partial r} \propto \mathbf{v}_0$. We see that $-\mathbf{H}(\boldsymbol{\zeta})\partial\boldsymbol{\zeta}$ needs to be proportional to $\mathbf{v}_0$, or equivalently $\partial\boldsymbol{\zeta} \propto -\mathbf{H}(\boldsymbol{\zeta})^{-1}\mathbf{v}_0$. Regularizing with respect to r, we get $\frac{\partial \boldsymbol{\zeta}}{\partial r} = -\mathbf{H}(\boldsymbol{\zeta})^{-1}\mathbf{v}_0(\boldsymbol{\eta}^\mathsf{T}\mathbf{H}(\boldsymbol{\zeta})^{-1}\mathbf{v}_0)^{-1}$. This derivative exists everywhere except at foci. Hence, $\boldsymbol{\xi}_{\mathbf{v}_0}$ is a curve that is regular everywhere except at foci. Furthermore, the set $\mathcal{U}_i$ contains the limit points of $\mathbf{v}(\mathbf{x})$ as $\mathbf{x} \to \mathbf{p}_i$. □

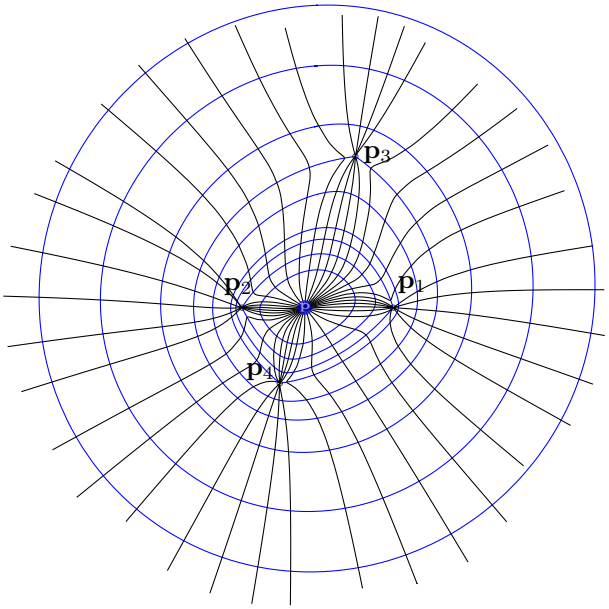

Figure 2: Multiple confocal 4-ellipsoids in 2-D with various isonormal curves $\boldsymbol{\xi}_{\mathbf{v}_0}$ corresponding to $\mathbf{v}_0 = [\cos(\theta), \sin(\theta)]^\mathsf{T}$ for $\theta \in \{\frac{i\pi}{18}\}_{i=0}^{35}$. Point Ⓟ is the geometric median of foci.

Figures 1d and 1e have the $\boldsymbol{\xi}_{\mathbf{v}^*}, \boldsymbol{\xi}_{-\mathbf{v}^*}$ curves for $k = 2, 3$. Fig. 2 depicts these curves for different unit vectors $\mathbf{v}_0$ with $k = 4$. See [8, Fig. 2] for a similar plot for $k = 3$.

Remark 2. *Since the unstable equilibrium points of $\boldsymbol{f}_t$ lie on the $\boldsymbol{\xi}_{-\mathbf{v}^*}$ curve, $\boldsymbol{f}_t$ is almost globally stable, except on the 1-D set $\boldsymbol{\xi}_{-\mathbf{v}^*}$ which has a Lebesgue measure zero.*

C. Combined Flow

We use the normalized fields $\boldsymbol{f}_n^\circ, \boldsymbol{f}_t^\circ$ instead of $\boldsymbol{f}_n, \boldsymbol{f}_t$ as their directions carry useful information while we manually set the magnitudes. Our goal is to build a combined field $\boldsymbol{f}$ from $\boldsymbol{f}_n^\circ, \boldsymbol{f}_t^\circ$ that converges to the intersection of $\partial\mathcal{D}^*$ and $\boldsymbol{\xi}_{\mathbf{v}^*}$ which is $\mathbf{x}^*$. We achieve this by a linear combination:

$$\boldsymbol{f}(\mathbf{x}) \doteq g_t(\mathbf{x})\boldsymbol{f}_t^\circ(\mathbf{x}) + g_n(\mathbf{x})\boldsymbol{f}_n^\circ(\mathbf{x}), \tag{13}$$

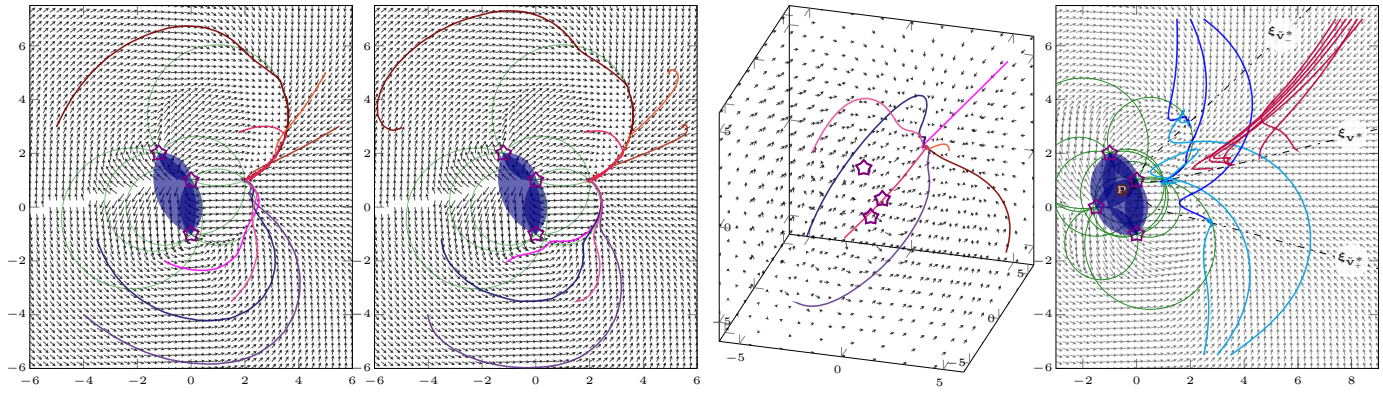

(a) Double integrator, $\lambda_0 = 1, \alpha = \frac{1}{4}$ (b) Unicycle, $k_v = 1, k_\omega = 2$ (c) Double integrator, $\lambda_0 = 1, \alpha = \frac{1}{4}$ (d) Double integrator, $\lambda_0 = \lambda_0 = 1$, $\lambda_0 = 0.7, \alpha = \frac{1}{4}$

Figure 3: In (a)-(b)-(c), trajectories of a double integrator and a unicycle and $\boldsymbol{f}(\mathbf{x})$ are given with respect to 3 landmarks from different starting points in 2D and 3D. The goal positions are located at $\mathbf{x}^* = [2,1]^\mathsf{T}$ and $\mathbf{x}^* = [2,1,2]^\mathsf{T}$. In (d), blue and cyan trajectories are convergent to $\mathbf{x}^* = [1,1]^\mathsf{T}$ and two other points at the intersection of $\partial\mathcal{D}^*$ and $\boldsymbol{\xi}_{\tilde{\mathbf{v}}^*_+}, \boldsymbol{\xi}_{\tilde{\mathbf{v}}^*_-}$, due to $\{0, \pm\frac{\pi}{6}\}$ radian tilt in the respective orientation frames. Purple trajectories correspond to six possible pairwise permutations of two of the bearings due to landmark mismatch, which all end on $\boldsymbol{\xi}_{\mathbf{v}^*}$ and outside of the obstacle sets, but not on $\mathbf{x}^*$.

where $g_t, g_n : \mathbb{R}^d \mapsto \mathbb{R}$ are non-negative *gain functions*.

Theorem 3. *The flow $\boldsymbol{f}$ almost globally converges to $\mathbf{x}^*$ if $g_t + g_n = 0$ only at $\mathbf{x}^*$ and $\sqrt{1 + \frac{g_n^2}{g_t^2}}\cos(\phi_{FOV} + \phi_0) > -1$ where $\phi_0 = \arctan(\frac{g_n}{g_t})$.*

Proof. From Theorem 2, $\dot{V}_t \propto -\boldsymbol{f}_t^\mathsf{T}\mathbf{H}\boldsymbol{f}$. Defining r_i as $r_i \doteq \|\mathbf{x} - \mathbf{p}_i\|$ and expanding $\mathbf{H}, \boldsymbol{f}$, we get $\dot{V}_t \propto -(\sum_{i=1}^k r_i^{-1}\boldsymbol{f}_t - \sum_{i=1}^k \frac{\mathbf{u}_i^\mathsf{T}\boldsymbol{f}_t}{r_i}\mathbf{u}_i)^\mathsf{T}\boldsymbol{f} = g_t\|\boldsymbol{f}_t\|\big(\sum_{i=1}^k r_i^{-1}((\mathbf{u}_i^\mathsf{T}\boldsymbol{f}_t^\circ)^2 - 1)\big) + g_n\|\boldsymbol{f}_t\|\big(\sum_{i=1}^k r_i^{-1}(\mathbf{u}_i^\mathsf{T}\boldsymbol{f}_t^\circ)(\mathbf{u}_i^\mathsf{T}\boldsymbol{f}_n^\circ)\big)$ which further simplifies to $\dot{V}_t \propto -g_t\|\boldsymbol{f}_t\|\sum_{i=1}^k r_i^{-1}\big(1 - (\mathbf{u}_i^\mathsf{T}\boldsymbol{f}_t^\circ)^2 - \frac{g_n}{g_t}(\mathbf{u}_i^\mathsf{T}\boldsymbol{f}_t^\circ)(\mathbf{u}_i^\mathsf{T}\boldsymbol{f}_n^\circ)\big)$. Since bearings are contained in a cone, we have $|\mathbf{u}_i^\mathsf{T}\boldsymbol{f}_n^\circ| \geq \cos(\frac{\phi_{\text{FOV}}}{2})$ and $\mathbf{u}_i^\mathsf{T}\boldsymbol{f}_t^\circ \leq \sin(\frac{\phi_{\text{FOV}}}{2})$, which gives $1 - (\mathbf{u}_i^\mathsf{T}\boldsymbol{f}_t^\circ)^2 - \frac{g_n}{g_t}(\mathbf{u}_i^\mathsf{T}\boldsymbol{f}_t^\circ)(\mathbf{u}_i^\mathsf{T}\boldsymbol{f}_n^\circ) \geq 1 - \sin^2(\frac{\phi_{\text{FOV}}}{2}) - \frac{g_n}{g_t}\sin(\frac{\phi_{\text{FOV}}}{2})\cos(\frac{\phi_{\text{FOV}}}{2}) = \frac{1}{2}(1 + \cos(\phi_{\text{FOV}}) - \frac{g_n}{g_t}\sin(\phi_{\text{FOV}})) = \frac{1}{2}(1 + \sqrt{1 + \frac{g_n^2}{g_t^2}}\cos(\phi_{\text{FOV}} + \phi_0))$ where $\phi_0 = \arctan(\frac{g_n}{g_t})$. Hence, it suffices for $\dot{V}_t < 0$ to have $\sqrt{1 + \frac{g_n^2}{g_t^2}}\cos(\phi_{\text{FOV}} + \phi_0) > -1$. Even if this is not met and $g_n\boldsymbol{f}_n^\circ$ momentarily increases V_t, the $g_t\boldsymbol{f}_t^\circ$ is eventually able to compensate thanks to its global stability. Moreover, since $\boldsymbol{f}_t$ keeps $\vartheta_\mathcal{P}$ fixed, the flow $g_n\boldsymbol{f}_n^\circ$ converges to $\partial\mathcal{D}^*$. □

While there is not a unique way to design these functions depending on the desired behaviour, we suggest these criteria:

1) The field $\boldsymbol{f}_t^\circ$ is always active.
2) If $\mathbf{x} \notin \mathcal{D}^*$, move towards $\partial\mathcal{D}^*$ by activating $\boldsymbol{f}_n^\circ$.
3) If $\mathbf{x} \in \mathcal{D}^*$, activate $\boldsymbol{f}_n^\circ$ only if $\mathbf{v}$ is close to $\mathbf{v}^*$.

The reason behind delayed activation of $\boldsymbol{f}_n^\circ$ when the robot is in $\mathcal{D}^*$ is that staying on $\partial\mathcal{D}^*$ might take the robot too close to the landmarks and cause collision, whereas staying on a k-ellipsoid in $\mathcal{D}^*$ ensures a minimum distance (see Fig. 1).

For smooth transitions, we use the smooth bump function:

$$b_\epsilon(x) \doteq \begin{cases} 0 & x < 0 \\ 3\epsilon^{-2}x^2 - 2\epsilon^{-3}x^3 & 0 \leq x \leq \epsilon \\ 1 & \epsilon < x \end{cases} \tag{14}$$

where ϵ is a design parameter. Our suggested functions are:

$$g_t(\mathbf{x}) \doteq \min(1, \sqrt{1 - \mathbf{v}^\mathsf{T}\mathbf{v}^*}) \tag{15a}$$
$$g_n(\mathbf{x}) \doteq \max(0, \mathbf{v}^\mathsf{T}\mathbf{v}^*)b_\epsilon(\delta_{\hat{\imath}\hat{\jmath}}) + b_\epsilon(-\delta_{\hat{\imath}\hat{\jmath}})\,. \tag{15b}$$

The function g_t is: *1)* equal to one when $\measuredangle(\mathbf{v}, \mathbf{v}^*) \geq \frac{\pi}{2}$, *2)* less than one when $\measuredangle(\mathbf{v}, \mathbf{v}^*) < \frac{\pi}{2}$, which slows down the convergence to $\mathbf{v}^*$ as $\mathbf{v} \to \mathbf{v}^*$. The function g_n: *1)* pushes the robot away if $\delta_{\hat{\imath}\hat{\jmath}}$ is negative by $b_\epsilon(-\delta_{\hat{\imath}\hat{\jmath}})$, *2)* attracts it towards the foci by $b_\epsilon(\delta_{\hat{\imath}\hat{\jmath}})\cos(\measuredangle(\mathbf{v}, \mathbf{v}^*))$ once $\measuredangle(\mathbf{v}, \mathbf{v}^*) < \frac{\pi}{2}$. Using a bump function will smoothen the transition of the normal flow at $\partial\mathcal{D}^*$. We choose ϵ such that $\epsilon < \min_{p,q} \mathbf{u}_p^{*\mathsf{T}}\mathbf{u}_q^* - \cos(\phi_{\text{FOV}})$ to ensures that the smooth transition phase never falls in the obstacle set $\mathcal{O}_{\hat{\imath}\hat{\jmath}}$. For such pair $\hat{p}, \hat{q}$ with $\tau = \mathbf{u}_{\hat{p}}^{*\mathsf{T}}\mathbf{u}_{\hat{q}}^* - \cos(\phi_{\text{FOV}})$, we have $b_\epsilon(-\delta_{\hat{p}\hat{q}}) = 1$ if $-\tau < \delta_{pq} \leq -\epsilon$.

Remark 3. *While the visual homing approaches typically require all of the desired bearings, $\boldsymbol{f}$ can be utilized using only the unit vector $\mathbf{v}^* \in \mathbb{S}^{d-1}$ (containing $d-1$ parameters) and the angle between the bearings of two of the desired landmarks (i.e. $\measuredangle(\mathbf{u}_i^*, \mathbf{u}_j^*)$). These d parameters produce a minimal representation of the home location $\mathbf{x}^*$ (See Fig. 1e).*

D. Failure Analysis

Landmark mismatch: As $\boldsymbol{f}_t$ only requires $\mathbf{v}, \mathbf{v}^*$ and these are obtained from unordered sums over the bearings (7), both $\mathbf{v}, \mathbf{v}^*$ can be computed without directly associating each bearing $\mathbf{u}_i$ with its corresponding $\mathbf{u}_i^*$. For $\boldsymbol{f}_n$, however, correct associations are needed for calculating $\{\delta_{ij}\}$ and $\delta_{\hat{\imath}\hat{\jmath}}$. If bearings are mismatched, the convergent point $\tilde{\mathbf{x}}^*$ still lies on $\boldsymbol{\xi}_{\mathbf{v}^*}$ as $\boldsymbol{f}_t$ remains the same, but $\tilde{\mathbf{x}}^* \neq \mathbf{x}^*$ if $\hat{\imath}$ or $\hat{\jmath}$ is mismatched near $\tilde{\mathbf{x}}^*$. Point $\tilde{\mathbf{x}}^*$ is not inside of obstacle sets nonetheless since the angle between any pair of desired bearings is less than ϕ_{FOV}.

Occlusion: If sight over some of the landmarks is lost due to occlusion, the combined flow of the remaining landmarks remains convergent to $\mathbf{x}^*$ (See Fig. 1 for $k = 3, 2$). Notice that $\boldsymbol{f}_t$ only needs a single landmark, but $\boldsymbol{f}_n$ needs at least two.

Orientation bias: If there is bias in the orientation estimate of the robot with respect to a global frame in which $\{\mathbf{u}_{ij}^*\}$ are expressed, the bearing measurements $\tilde{\mathbf{u}}_{ij}$ are corrupted by a rotation $\tilde{\mathbf{R}} \in \mathrm{SO}(d)$ such that $\tilde{\mathbf{u}_{ij}} = \tilde{\mathbf{R}}\mathbf{u}_{ij}$. In this case, the combined flow is convergent to the intersection of $\partial\mathcal{D}^*$ and $\boldsymbol{\xi}_{\tilde{\mathbf{v}}^*}$, where $\tilde{\mathbf{R}}\tilde{\mathbf{v}}^* = \mathbf{v}^*$ or $\tilde{\mathbf{v}}^* = \tilde{\mathbf{R}}^\mathsf{T}\mathbf{v}^*$.

IV. APPLICATIONS BEYOND SINGLE INTEGRATORS

Following [18], we propose control laws for double integrator and unicycle dynamics. We empirically show via simulations the convergence of these applied control laws. A full theoretical convergence analysis (e.g. the basin of attraction of initial conditions) is left out of the scope of this paper.

A. Double Integrator Control Synthesis

We assume the following linear system dynamics:

$$\ddot{\mathbf{x}} = -\lambda_0\dot{\mathbf{x}} + \boldsymbol{\mu}, \quad \boldsymbol{\mu} = \alpha\boldsymbol{f}(\mathbf{x}), \tag{16}$$

where $\mathbf{x} \in \mathbb{R}^d$ is the position, $\alpha > 0$ is a constant, and $\lambda_0 > 0$ is a damping coefficient. An appropriate choice of λ_0 is necessary to alleviate overshoots.

B. Unicycle Control Synthesis

Instead of $\boldsymbol{f}$ we use $\boldsymbol{f}^\circ$ as a *navigation function*, which suggests the suitable direction to follow, and requires manual setting of the velocities (as in [18]). For the state variables $\mathbf{q} = [\,\mathbf{x}^\mathsf{T}, \theta\,]^\mathsf{T} \in \mathbb{R}^3$ consisting of the position $\mathbf{x} \in \mathbb{R}^2$ and the orientation θ, the equations of motion are:

$$\dot{\mathbf{q}} = [\,\cos(\theta) \quad \sin(\theta) \quad 0\,]^\mathsf{T}\upsilon + [\,0 \quad 0 \quad 1\,]^\mathsf{T}\omega\,, \tag{17}$$

where $\upsilon, \omega \in \mathbb{R}$ are linear and angular velocities of the robot with respect to its body-fixed frame. Given the following:

$$\upsilon = k_\upsilon\big(\sqrt{1 - \mathbf{v}^\mathsf{T}\mathbf{v}^*} + |\delta_{\hat{\imath}\hat{\jmath}}|\big) \tag{18a}$$

$$\omega = -k_\omega(\theta - \psi) + \dot{\psi} \tag{18b}$$

as suggested control law, $\psi \doteq \arctan(f_2^\circ, f_1^\circ)$ is the orientation of $\boldsymbol{f}^\circ(\mathbf{x})$ at current position and k_υ, k_ω are positive gains. In (18a), the velocity is positive everywhere except at $\mathbf{x}^*$, and (18b) yields exponential convergence of θ to ψ.

V. SIMULATION RESULTS

We present simulation results for the visual homing problem for unicycles in 2D and double integrators in 2D and 3D. In Fig. 3, the trajectories from control laws in (16) and (18) are plotted from different initial states. See [9] for more results.

VI. CONCLUSIONS

We presented a novel navigational vector field suitable for controlling double integrators and unicycles for the visual homing problem. Our vector field works with a minimal representation of the home location, and is almost globally stable while respecting field of view constraints. An interesting future direction is to use our vector field in the formation control problem along with control barrier functions. Another direction is finding a feasible point to gain back vision over landmarks when robot hits an FOV obstacle.

REFERENCES

[1] A. A. Argyros, K. E. Bekris, and S. C. Orphanoudakis. Robot homing based on corner tracking in a sequence of panoramic images. In *Proceedings of the 2001 IEEE Computer Society Conference on Computer Vision and Pattern Recognition. CVPR 2001*, volume 2. IEEE, 2001.

[2] C. I. Connolly, J. B. Burns, and R. Weiss. Path planning using laplace's equation. In *Proceedings., IEEE International Conference on Robotics and Automation*, pages 2102–2106. IEEE, 1990.

[3] P. Corke. Mobile robot navigation as a planar visual servoing problem. In *Robotics Research*, pages 361–372. Springer, 2003.

[4] N. J. Cowan, J. D. Weingarten, and D. E. Koditschek. Visual servoing via navigation functions. *IEEE Transactions on Robotics and Automation*, 18(4):521–533, 2002.

[5] K. F. Gauss and P. Pesic. *General investigations of curved surfaces*. Courier Corporation, 2005.

[6] E. G. Hernández-Martínez, E. Aranda-Bricaire, F. Alkhateeb, E. Maghayreh, and I. Doush. *Convergence and collision avoidance in formation control: A survey of the artificial potential functions approach*. INTECH Open Access Publisher Rijeka, Croatia, 2011.

[7] J. Hong, X. Tan, B. Pinette, R. Weiss, and E. M. Riseman. Image-based homing. *IEEE Control Systems Magazine*, 12(1):38–45, 1992.

[8] A. Karimian and R. Tron. Bearing-only consensus and formation control under directed topologies. In *2020 American Control Conference (ACC)*, pages 3503–3510. IEEE, 2020.

[9] A. Karimian and R. Tron. Bearing-only navigation with field of view constraints. *arXiv preprint arXiv:2009.07308*, 2020.

[10] O. Khatib. Real-time obstacle avoidance for manipulators and mobile robots. In *Autonomous robot vehicles*, pages 396–404. Springer, 1986.

[11] J.-O. Kim and P. Khosla. Real-time obstacle avoidance using harmonic potential functions. 1992.

[12] D. Lambrinos, R. Möller, R. Pfeifer, and R. Wehner. Landmark navigation without snapshots: the average landmark vector model. In *Proc. Neurobiol. Conf. Göttingen*, 1998.

[13] J. Lim, N. Barnes, et al. Robust visual homing with landmark angles. In *Robotics: science and systems*, 2009.

[14] M. Liu, C. Pradalier, Q. Chen, and R. Siegwart. A bearing-only 2d/3d-homing method under a visual servoing framework. In *2010 IEEE International Conference on Robotics and Automation*, pages 4062–4067. IEEE, 2010.

[15] M. Liu, C. Pradalier, and R. Siegwart. Visual homing from scale with an uncalibrated omnidirectional camera. *IEEE Transactions on Robotics*, 29(6):1353–1365, 2013.

[16] S. G. Loizou and V. Kumar. Biologically inspired bearing-only navigation and tracking. In *2007 46th IEEE Conference on Decision and Control*, pages 1386–1391. IEEE, 2007.

[17] G. López-Nicolás, N. R. Gans, S. Bhattacharya, C. Sagues, J. J. Guerrero, and S. Hutchinson. Homography-based control scheme for mobile robots with nonholonomic and field-of-view constraints. *IEEE Transactions on Systems, Man, and Cybernetics, Part B (Cybernetics)*, 40(4):1115–1127, 2009.

[18] D. Panagou. Motion planning and collision avoidance using navigation vector fields. In *2014 IEEE International Conference on Robotics and Automation (ICRA)*, pages 2513–2518. IEEE, 2014.

[19] D. Panagou. A distributed feedback motion planning protocol for multiple unicycle agents of different classes. *IEEE Transactions on Automatic Control*, 62(3):1178–1193, 2016.

[20] N. P. Papanikolopoulos and P. K. Khosla. Adaptive robotic visual tracking: Theory and experiments. *IEEE Transactions on Automatic Control*, 38(3):429–445, 1993.

[21] E. Rimon and D. E. Koditschek. Exact robot navigation using artificial potential functions. *Departmental Papers (ESE)*, page 323, 1992.

[22] R. Tron and K. Daniilidis. An optimization approach to bearing-only visual homing with applications to a 2-d unicycle model. In *2014 IEEE International Conference on Robotics and Automation (ICRA)*, pages 4235–4242. IEEE, 2014.

[23] Y. Vardi and C.-H. Zhang. The multivariate l1-median and associated data depth. *Proceedings of the National Academy of Sciences*, 97(4):1423–1426, 2000.